Mechanical bidomain model of cardiac muscle with unequal anisotropy ratios

Dilmini Wijesinghe and Bradley J. Roth
Department of Physics, Oakland University, Rochester, Michigan 48309, USA

(Received 11 September 2019; published 26 December 2019)

The properties of cardiac muscle are anisotropic, and the degree of anisotropy may be different in the intracellular and extracellular spaces. In the electrical bidomain model, such "unequal anisotropy ratios" of the conductivity lead to unanticipated behavior. In the mechanical bidomain model, unequal anisotropy ratios of the mechanical moduli might also result in unanticipated behavior. In this study, mathematical modeling based on the mechanical bidomain model is used to calculate the distribution of mechanotransduction in cardiac tissue when it is stretched. This analysis demonstrates that unexpected phenomena arise when the mechanical anisotropy ratios are unequal.

DOI: 10.1103/PhysRevE.100.062417

I. INTRODUCTION

Cardiac tissue is anisotropic [1–3] and the fiber geometry throughout the heart is complicated [4,5]. Growth and remodeling of the heart may be influenced by mechanical forces and mechanotransduction [6–9]. Therefore, anisotropy is crucial for understanding the behavior of the heart.

The effects of anisotropy on cardiac tissue have been discussed using the *electrical* bidomain model, a macroscopic model that describes the bioelectric behavior of the heart [10]. In the electrical bidomain model, the tissue is considered as a continuum of two phases; extracellular and intracellular separated by a membrane. It calculates the electrical potential in the intra- and extracellular spaces, and the differences between the two: the transmembrane potential. Sepulveda *et al.* [11] used the electrical bidomain model to analyze anisotropic cardiac tissue and observed complex spatial distributions of current and potential with depolarized and hyperpolarized areas adjacent to an externally applied cathode. They found that these unusual spatial distributions were due to "unequal anisotropy ratios;" the anisotropy of the electrical conductivity was different in the intra- and extracellular spaces. Many other behaviors become apparent only when tissue has unequal anisotropy [12].

In the last ten years, a *mechanical* version of the bidomain model was developed to study mechanotransduction [13]. It calculates displacements in the intra- and extracellular spaces, and the differences between the two: the force on integrin proteins. These membrane proteins are known to play a crucial role during mechanotransduction in the heart [14–16]. The key hypothesis of the mechanical bidomain model is that the difference of displacements of intra- and extracellular spaces gives rise to mechanotransduction [17]. Like the electrical conductivity, the mechanical modulus can be anisotropic, and may have different degrees of anisotropy in the intra- and extracellular spaces.

In this paper we analyze the mechanical behavior of cardiac tissue when it has unequal anisotropy ratios. We derive the equations of the mechanical bidomain model that predict where mechanotransduction occurs when the anisotropies of the mechanical properties are different in the intra- and extracellular spaces. Our goal is to determine if—as for the electrical bidomain model—unexpected behavior arises when the mechanical anisotropy ratios are unequal.

II. METHODS

A. Derivation of analytical equations

We analyze a two-dimensional sheet of anisotropic cardiac tissue using the mechanical bidomain model. The intracellular and extracellular spaces are coupled by integrins, a transmembrane protein that connects the cytoskeleton to the extracellular matrix [16]. The two spaces and the integrins are represented by springs obeying Hooke's law. The intracellular and extracellular displacements are denoted by **u** and **w**. The difference between the displacement of the two spaces (**u**-**w**) causes a mechanical force that activates the integrins.

Before deriving the mechanical equations in detail, we outline the derivation. First, we propose stress-strain relationships for the intra- and extracellular spaces individually. Then we assume incompressibility and mechanical equilibrium to obtain equations governing the intra- and extracellular stream functions that determine uniquely the displacements. Finally, the equations simplify if, instead of expressing them in terms of intra- and extracellular stream functions, we introduce "monodomain" and "bidomain" stream functions. In particular the bidomain stream function is important, because the bidomain displacement causes forces on integrins.

The tissue is anisotropic, having different mechanical properties along and across the fibers. The direction of the curved fiber distribution is specified by the angle of the fibers with the x axis, $\theta(x, y)$. The isotropic part of the tissue properties is characterized by intra- and extracellular shear moduli, ν and μ. Anisotropy is included as an additional Young's modulus along the fiber axis in the intracellular (γ_i) and extracellular (γ_e) spaces.

We consider an incompressible tissue since tissue is mostly water. The relationships between intracellular stress (τ) and

 ©2019 American Physical Society

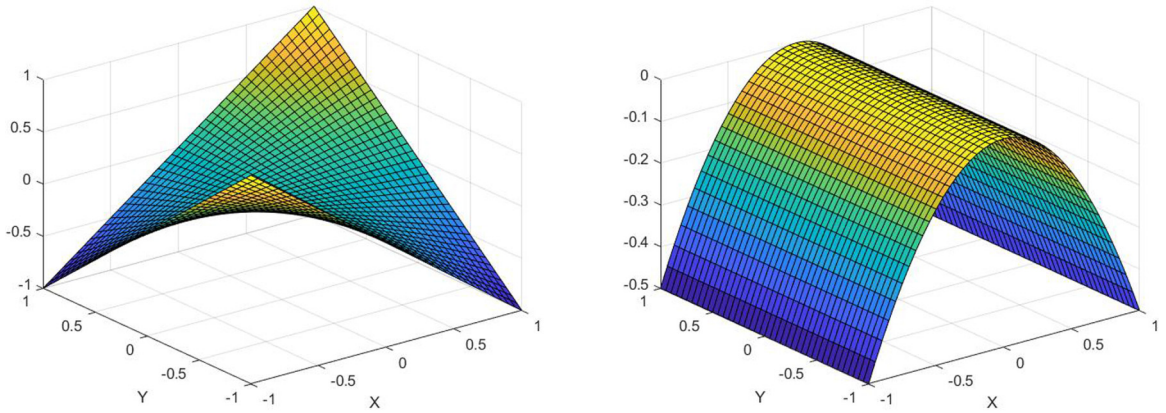

FIG. 1. The monodomain stream function as a function of X and Y, for isotropic tissue. (a) $\psi = XY$ (uniaxial stretch) and (b) $\psi = -\frac{X^2}{2}$ (shear).

strain (ε) tensors are

$$\tau_{ixx} = -p + 2\nu\varepsilon_{ixx} + \gamma_i(\varepsilon_{ixx}\cos^4\theta + 2\varepsilon_{ixy}\sin\theta\cos^3\theta + \varepsilon_{iyy}\sin^2\theta\cos^2\theta), \quad (1)$$

$$\tau_{iyy} = -p + 2\nu\varepsilon_{iyy} + \gamma_i(\varepsilon_{ixx}\cos^2\theta\sin^2\theta + 2\varepsilon_{ixy}\sin^3\theta\cos\theta + \varepsilon_{iyy}\sin^4\theta), \quad (2)$$

$$\tau_{ixy} = 2\nu\varepsilon_{ixy} + \gamma_i(\varepsilon_{ixx}\sin\theta\cos^3\theta + 2\varepsilon_{ixy}\sin^2\theta\cos^2\theta + \varepsilon_{iyy}\sin^3\theta\cos\theta). \quad (3)$$

The final terms multiplied by γ_i arise from the stress along the fibers in the fiber coordinate system, transformed into the lab coordinate system. Similarly, the stress and strain relationships for the extracellular space are

$$\tau_{exx} = -q + 2\mu\varepsilon_{exx} + \gamma_e(\varepsilon_{exx}\cos^4\theta + 2\varepsilon_{exy}\sin\theta\cos^3\theta + \varepsilon_{eyy}\sin^2\theta\cos^2\theta), \quad (4)$$

$$\tau_{eyy} = -q + 2\mu\varepsilon_{eyy} + \gamma_e(\varepsilon_{exx}\cos^2\theta\sin^2\theta + 2\varepsilon_{exy}\sin^3\theta\cos\theta + \varepsilon_{eyy}\sin^4\theta), \quad (5)$$

$$\tau_{exy} = 2\mu\varepsilon_{exy} + \gamma_e(\varepsilon_{exx}\sin\theta\cos^3\theta + 2\varepsilon_{exy}\sin^2\theta\cos^2\theta + \varepsilon_{eyy}\sin^3\theta\cos\theta), \quad (6)$$

where p and q are the hydrostatic pressure of the intra- and extracellular spaces.

Linear strains can be expressed in terms of the displacements of intra- and extracellular spaces, **u** and **w**,

$$\varepsilon_{ixx} = \frac{\partial u_x}{\partial x}, \quad \varepsilon_{iyy} = \frac{\partial u_y}{\partial y}, \quad \varepsilon_{ixy} = \frac{1}{2}\left(\frac{\partial u_x}{\partial y} + \frac{\partial u_y}{\partial x}\right), \quad (7)$$

$$\varepsilon_{exx} = \frac{\partial w_x}{\partial x}, \quad \varepsilon_{eyy} = \frac{\partial w_y}{\partial y}, \quad \varepsilon_{exy} = \frac{1}{2}\left(\frac{\partial w_x}{\partial y} + \frac{\partial w_y}{\partial x}\right). \quad (8)$$

The displacements have zero divergence because the tissue is incompressible. Using stream functions ϕ and η, we can write down the intracellular and extracellular displacements as

$$u_x = \frac{\partial\phi}{\partial y}, \quad u_y = -\frac{\partial\phi}{\partial x}, \quad w_x = \frac{\partial\eta}{\partial y}, \quad w_y = -\frac{\partial\eta}{\partial x}. \quad (9)$$

The four equations of the mechanical equilibrium are

$$\frac{\partial\tau_{ixx}}{\partial x} + \frac{\partial\tau_{ixy}}{\partial y} = K(u_x - w_x), \quad (10)$$

$$\frac{\partial\tau_{ixy}}{\partial x} + \frac{\partial\tau_{iyy}}{\partial y} = K(u_y - w_y), \quad (11)$$

$$\frac{\partial\tau_{exx}}{\partial x} + \frac{\partial\tau_{exy}}{\partial y} = -K(u_x - w_x), \quad (12)$$

$$\frac{\partial\tau_{exy}}{\partial x} + \frac{\partial\tau_{eyy}}{\partial y} = -K(u_y - w_y). \quad (13)$$

These equations imply that the sum of the forces in each space is zero. As an example, in the intracellular space the forces in the x direction can be found by taking the divergence of the intracellular stress tensor, and including a term representing the coupling between the two spaces by the integrins [18]. The parameter K indicates the spring constant of the coupling.

By substituting Eqs. (1)–(9) into the four equations of mechanical equilibrium, Eqs. (10)–(13), we obtain four equations for the forces in the intra- and extracellular spaces. The two equations of the intracellular space are

$$-\frac{\partial p}{\partial x} + \nu\left(\frac{\partial^3\phi}{\partial x^2\partial y} + \frac{\partial^3\phi}{\partial y^3}\right) + \frac{\gamma_i}{8}\left\{(1 + 3\cos 4\theta + 4\cos 2\theta)\frac{\partial^3\phi}{\partial x^2\partial y} + (3\sin 4\theta + 2\sin 2\theta)\frac{\partial^3\phi}{\partial x\partial y^2}\right.$$
$$-\left[(8\sin 4\theta + 8\sin 2\theta)\frac{\partial\theta}{\partial x} - 8\cos 4\theta\frac{\partial\theta}{\partial y}\right]\frac{\partial^2\phi}{\partial x\partial y} - (\sin 4\theta + 2\sin 2\theta)\frac{\partial^3\phi}{\partial x^3} + (1 - \cos 4\theta)\frac{\partial^3\phi}{\partial y^3}$$
$$\left.+\left[4\sin 4\theta\frac{\partial\theta}{\partial y} + (4\cos 4\theta + 4\cos 2\theta)\frac{\partial\theta}{\partial x}\right]\left(\frac{\partial^2\phi}{\partial y^2} - \frac{\partial^2\phi}{\partial x^2}\right)\right\} = K\left(\frac{\partial\phi}{\partial y} - \frac{\partial\eta}{\partial y}\right), \quad (14)$$

$$-\frac{\partial p}{\partial y} - \nu\left(\frac{\partial^3\phi}{\partial x\partial y^2} + \frac{\partial^3\phi}{\partial x^3}\right) + \frac{\gamma_i}{8}\left\{(3\sin 4\theta - 2\sin 2\theta)\frac{\partial^3\phi}{\partial x^2\partial y} + (-1 - 3\cos 4\theta + 4\cos 2\theta)\frac{\partial^3\phi}{\partial x\partial y^2}\right.$$
$$+\left[8\cos 4\theta\frac{\partial\theta}{\partial x} + (8\sin 4\theta - 8\sin 2\theta)\frac{\partial\theta}{\partial y}\right]\frac{\partial^2\phi}{\partial x\partial y} - (1-\cos 4\theta)\frac{\partial^3\phi}{\partial x^3} - (\sin 4\theta - 2\sin 2\theta)\frac{\partial^3\phi}{\partial y^3}$$
$$\left.+\left[4\sin 4\theta\frac{\partial\theta}{\partial x} - (4\cos 4\theta - 4\cos 2\theta)\frac{\partial\theta}{\partial y}\right]\left(\frac{\partial^2\phi}{\partial y^2} - \frac{\partial^2\phi}{\partial x^2}\right)\right\} = -K\left(\frac{\partial\phi}{\partial x} - \frac{\partial\eta}{\partial x}\right). \tag{15}$$

Similarly, we can derive two equations for the extracellular space.

Next, we introduce two stream functions λ and ψ,

$$\lambda = \phi - \eta, \tag{16}$$

$$\psi = \phi + \frac{\mu}{\nu}\eta. \tag{17}$$

These stream functions simplify the set of derived equations [18]. The stream function λ describes the bidomain behavior (the difference between the two spaces) and therefore specifies where there are forces on integrins. The stream function ψ describes the monodomain behavior (a weighted average of the two spaces). The specific weighting is chosen so that the final equations, Eqs. (20) and (21), uncouple under the condition of equal anisotropy ratios.

In addition to the stream functions, we introduce a set of dimensionless parameters,

$$X = \frac{x}{D}, \quad Y = \frac{y}{D}, \quad \varepsilon = \left(\frac{\sigma}{D}\right)^2, \tag{18}$$

where D is a length characteristic of the tissue (in our case, it is the length of a side of the tissue sheet), and σ is the length constant that commonly arises in the mechanical bidomain model [17]:

$$\sigma = \sqrt{\frac{\nu\mu}{K(\nu+\mu)}}. \tag{19}$$

We manipulate the two intracellular equations, Eqs. (14) and (15), in such a way that the hydrostatic pressure p is eliminated, i.e., by taking the difference of the Y derivative of Eq. (14) and the X derivative of Eq. (15). Similarly, the hydrostatic pressure q can be eliminated from the two equations for the extracellular space. This leads to a system of coupled equations for ψ and λ,

$$\nabla^4\psi + \frac{(\gamma_i + \gamma_e)}{8(\nu+\mu)}\hat{f}\psi + \frac{(\mu\gamma_i - \nu\gamma_e)}{8\nu(\nu+\mu)}\hat{f}\lambda = 0, \tag{20}$$

$$\nabla^4\lambda + \frac{(\mu^2\gamma_i + \nu^2\gamma_e)}{8\mu\nu(\nu+\mu)}\hat{f}\lambda + \frac{(\mu\gamma_i - \nu\gamma_e)}{8\mu(\nu+\mu)}\hat{f}\psi = \frac{1}{\varepsilon}\nabla^2\lambda, \tag{21}$$

where the operator $\hat{f}$ is

$$\hat{f} = (6\cos 4\theta + 2)\frac{\partial^4}{\partial X^2\partial Y^2} + (1-\cos 4\theta)\left(\frac{\partial^4}{\partial X^4} + \frac{\partial^4}{\partial Y^4}\right) - \left(24\cos 4\theta\frac{\partial\theta}{\partial X} + 24\sin 4\theta\frac{\partial\theta}{\partial Y}\right)\frac{\partial^3}{\partial X^2\partial Y}$$
$$+\left(24\cos 4\theta\frac{\partial\theta}{\partial Y} - 24\sin 4\theta\frac{\partial\theta}{\partial X}\right)\frac{\partial^3}{\partial X\partial Y^2} + \left(8\sin 4\theta\frac{\partial\theta}{\partial Y} + 8\cos 4\theta\frac{\partial\theta}{\partial X}\right)\frac{\partial^3}{\partial Y^3} + \left(8\sin 4\theta\frac{\partial\theta}{\partial X} - 8\cos 4\theta\frac{\partial\theta}{\partial Y}\right)\frac{\partial^3}{\partial X^3}$$
$$-4\sin 4\theta\left(\frac{\partial^4}{\partial X^3\partial Y} - \frac{\partial^4}{\partial X\partial Y^3}\right) - \left\{8\cos 4\theta\left(\frac{\partial^2\theta}{\partial X^2} - \frac{\partial^2\theta}{\partial Y^2}\right) + 16\sin 4\theta\frac{\partial^2\theta}{\partial X\partial Y} + 32\sin 4\theta\left[\left(\frac{\partial\theta}{\partial Y}\right)^2 - \left(\frac{\partial\theta}{\partial X}\right)^2\right]\right.$$
$$\left.+64\cos 4\theta\frac{\partial\theta}{\partial Y}\frac{\partial\theta}{\partial X}\right\}\frac{\partial^2}{\partial X\partial Y} + \left\{4\sin 4\theta\left(\frac{\partial^2\theta}{\partial Y^2} - \frac{\partial^2\theta}{\partial X^2}\right) + 8\cos 4\theta\frac{\partial^2\theta}{\partial X\partial Y} + 16\cos 4\theta\left[\left(\frac{\partial\theta}{\partial Y}\right)^2 - \left(\frac{\partial\theta}{\partial X}\right)^2\right]\right.$$
$$\left.-32\sin 4\theta\frac{\partial\theta}{\partial Y}\frac{\partial\theta}{\partial X}\right\}\left(\frac{\partial^2}{\partial Y^2} - \frac{\partial^2}{\partial X^2}\right). \tag{22}$$

The two partial differential equations, Eqs. (20) and (21), are a coupled system of equations governing the monodomain, ψ, and bidomain, λ, behavior. If $\mu\gamma_i - \nu\gamma_e$ is zero, the equations of the mechanical bidomain model uncouple in a way similar to the electrical bidomain model, and $\frac{\gamma_i}{\nu} \neq \frac{\gamma_e}{\mu}$ is analogous to the condition of unequal anisotropy ratios [12]. In our simulations, we will assume $\nu = \mu$, so the condition of unequal anisotropy ratios is $\gamma_i \neq \gamma_e$.

Note that in Eqs. (20) and (21) the four parameters ν, μ, γ_i, and γ_e can all be rescaled by a common factor and the equations remain unchanged. Therefore, we assume $\nu = \mu = 1$ and vary γ_i and γ_e. For isotropic tissue, $\gamma_i = \gamma_e = 0$. For anisotropic tissue with equal anisotropy ratios, $\gamma_i = \gamma_e = 1$. Finally, for the general case of unequal anisotropy ratios, $\gamma_i = 1$ and $\gamma_e = 0$.

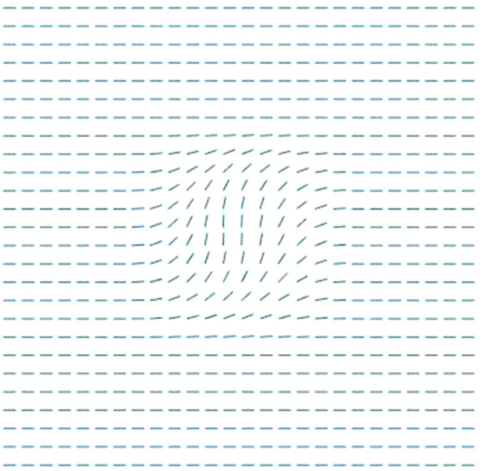

FIG. 2. The fiber distribution in a 2D sheet of cardiac tissue given by Eq. (23). X is horizontal and ranges from -1 to 1.

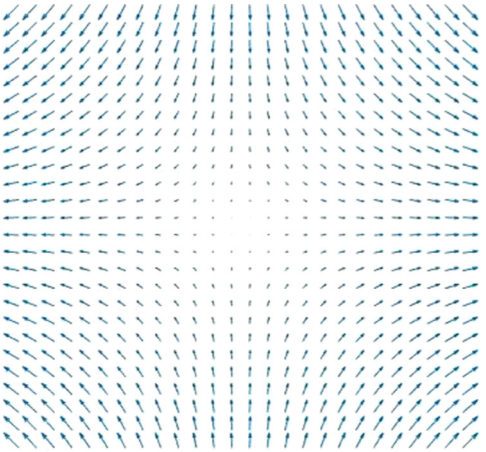

FIG. 3. Monodomain displacement **m** in isotropic tissue under uniaxial stretch. The fiber geometry $\theta(X, Y)$ is given by Eq. (23), the boundary conditions were applied using $\psi = XY$, and $\gamma_i = \gamma_e = 0$. The peak value of the monodomain displacement is 1 (in dimensionless units). Because $|\mathbf{m}|$ is much larger than $|\mathbf{b}|$ (see Fig. 5), a plot of **m** looks nearly identical to a plot of **u** or **w**.

B. Derivation of numerical equations

The coupled equations, Eqs. (20) and (21), are solved using the finite difference approximation and over-relaxation, an iterative technique. We considered a square grid with an equal space step in both directions [18,19].

Previous studies have examined how a boundary layer can form within a few length constants of the tissue surface [17,20]. In this study, we do not want to further examine that behavior, but rather want to focus on the effects of fiber curvature and unequal anisotropy ratios. Therefore, we introduce artificial boundary conditions: We set ψ at the boundary to a function that represents the limiting behavior of the monodomain far from the fiber direction heterogeneity, and set $\lambda = 0$ to eliminate any boundary layer.

We applied two different functions for the monodomain behavior ψ shown in Fig. 1. Figure 1(a) corresponds to normal strain with a magnitude of 1 and zero shear strain, as if the tissue were stretched in one direction (uniaxial stretch). Figure 1(b) corresponds to pure shear; the shear strain has a magnitude of $\frac{1}{2}$ and zero normal strain. The plots in Fig. 1 indicate how the stream functions behave throughout isotropic tissue, in which case ψ obeys the biharmonic equation $\nabla^4\psi = 0$. In our calculations with anisotropic tissue, at the boundary we set λ equal to zero and ψ equal to one of these assumed functions, and then calculate how ψ and λ behave in the interior.

We used a $N \times N$ grid in numerical calculations, where $N = 105$ (including four fictitious nodes to implement the boundary conditions). In the dimensionless variables X and Y, the sheet extended from $-1 < X < 1$ and $-1 < Y < 1$. Therefore, the space step (Δ) is 0.02. The value of ε depends on the coupling strength between the two spaces, and represents the relative size of the bidomain length constant σ and the length scale D. We set $\sigma = D/100$, implying $\varepsilon = 0.0001$.

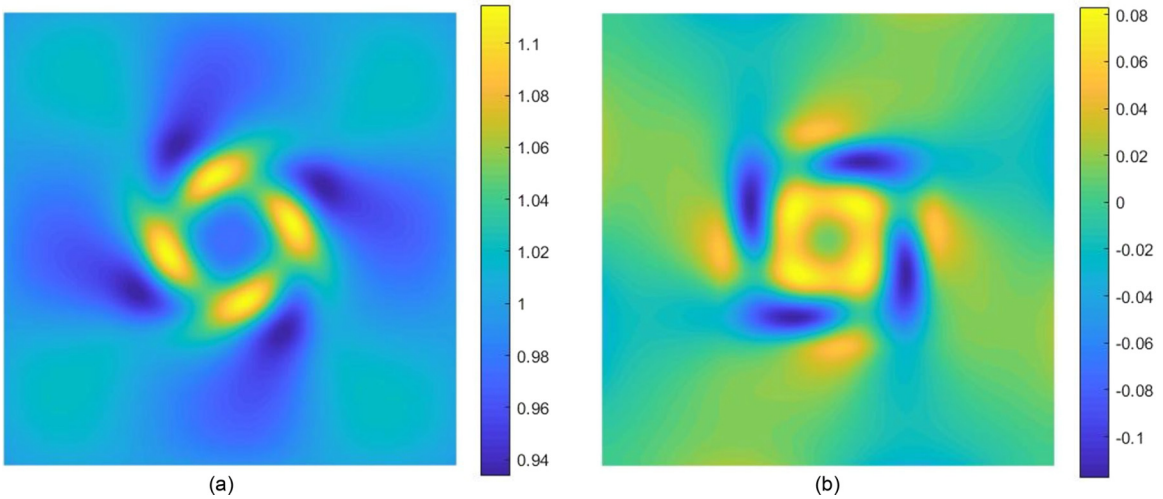

FIG. 4. Monodomain (a) normal strain and (b) shear strain for equal anisotropy ratios under uniaxial stretch. The fiber geometry $\theta(X, Y)$ is given by Eq. (23), boundary conditions were applied using $\psi = XY$, and $\gamma_i = \gamma_e = 1$.

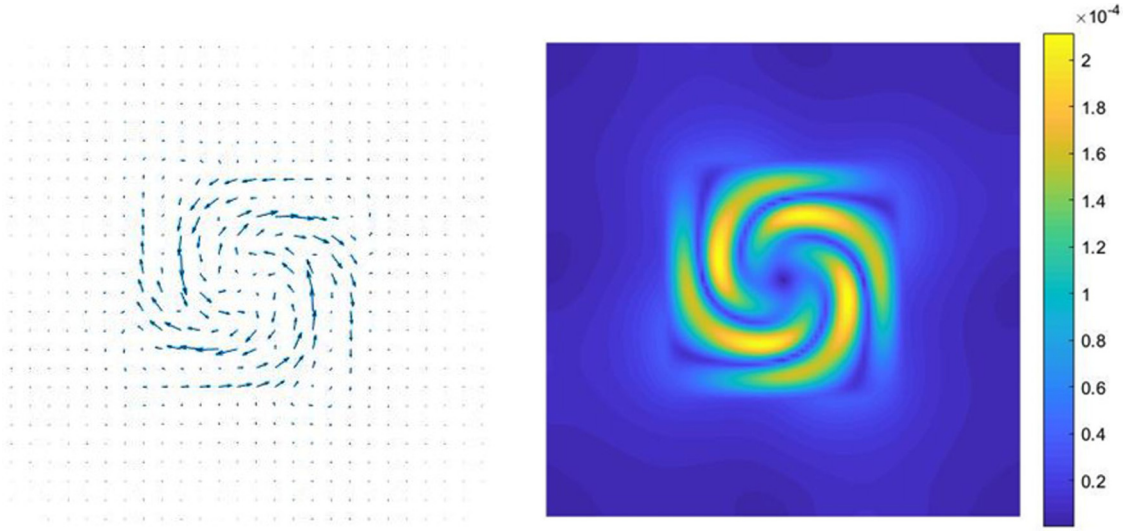

FIG. 5. (a) Bidomain displacement **b** in tissue with unequal anisotropy ratios under uniaxial stretch and (b) its magnitude $|\mathbf{b}|$. The fiber geometry $\theta(X, Y)$ is given by Eq. (23), boundary conditions were applied using $\psi = XY$, and $\gamma_i = 1$ and $\gamma_e = 0$. The length of the bidomain arrows in (a) is scaled differently than the length of the monodomain arrows in Fig. 3. The monodomain displacement is about 5000 times larger than the bidomain displacement.

III. RESULTS

A. Simple fiber geometry

As our first example, consider the fiber distribution given by the function

$$\theta(X, Y) = \frac{\pi}{2}\,(16X^4 - 8X^2 + 1)\,(16Y^4 - 8Y^2 + 1), \quad (23)$$

in the center region of the sheet ($-0.5 < X < 0.5$ and $-0.5 < Y < 0.5$) and $\theta(X, Y) = 0$ elsewhere, which leads to the simple fiber geometry shown in Fig. 2.

One virtue of this fiber geometry is that the fiber curvature is confined to a region near the center of the tissue, so we can avoid confusing effects caused by fiber curvature with effects arising at the tissue boundary. A similar fiber geometry was used in the analysis of the mechanical bidomain model with curving fibers that exert a tension [18], and in the analysis of the electrical bidomain model with curving fibers [21].

1. Uniaxial stretch

We define the monodomain, **m**, and bidomain, **b**, displacements as $\mathbf{m} = \mathbf{u} + \frac{\mu}{\nu}\,\mathbf{w}$ and $\mathbf{b} = \mathbf{u} - \mathbf{w}$ [18]. The X and Y components of the displacement vectors **m** and **b** are $m_x = \frac{\partial\psi}{\partial Y}$, $m_y = -\frac{\partial\psi}{\partial X}$, $b_x = \frac{\partial\lambda}{\partial Y}$, and $b_y = -\frac{\partial\lambda}{\partial X}$. Figure 3 shows the monodomain displacement for an isotropic tissue where $\gamma_i = \gamma_e = 0$, corresponding to a uniaxial stretching in the X direction with narrowing in the Y direction because of incompressibility. In this case the bidomain displacement **b** is zero. The monodomain normal strain is equal to 1 and is uniform throughout the tissue, and the monodomain shear strain is zero.

The monodomain displacement is changed only slightly when the tissue is anisotropic with equal anisotropy ratios ($\gamma_i = \gamma_e = 1$). A plot of **m** is nearly indistinguishable from that in Fig. 3. The bidomain displacement remains identically zero. The monodomain normal and shear strains, however, emphasize small deviations of the stream function caused by anisotropy, even for equal anisotropy ratios (Fig. 4). The magnitude of the normal strain varies by only about 10% from its value of 1 for isotropic tissue, and the shear strain is small (less than 0.1) throughout the sheet. The heterogeneities of the strains are largest where the fiber direction changes abruptly, but also spread throughout the tissue.

For unequal anisotropy ratios ($\gamma_i = 1$ and $\gamma_e = 0$), the monodomain displacement and strain appear similar to those

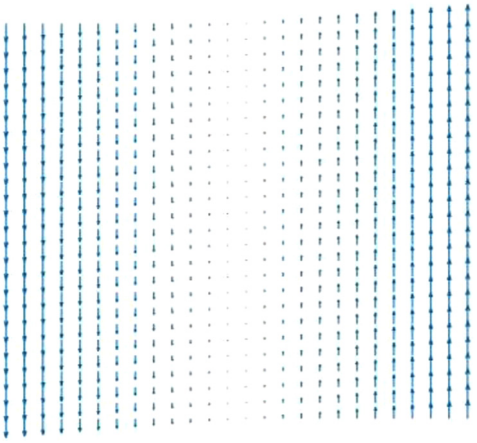

FIG. 6. Monodomain displacement **m**, in isotropic tissue under shear. The fiber geometry $\theta(X, Y)$ is given by Eq. (23), boundary conditions were applied using $\psi = -\frac{X^2}{2}$, and $\gamma_i = \gamma_e = 0$. The peak value of the monodomain displacement is 1 (in dimensionless units). Because $|\mathbf{m}|$ is much larger than $|\mathbf{b}|$ (see Fig. 8), a plot of **m** looks nearly identical to a plot of **u** or **w**.

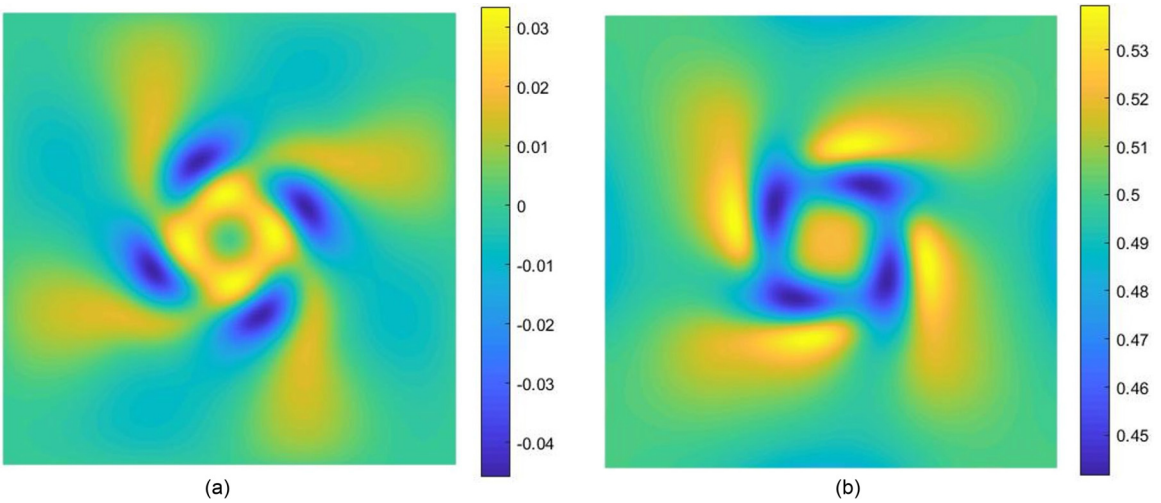

FIG. 7. Monodomain (a) normal strain and (b) shear strain for equal anisotropy ratios undergoing shear. The fiber geometry $\theta(X, Y)$ is given by Eq. (23), boundary conditions were applied using $\psi = -\frac{X^2}{2}$, and $\gamma_i = \gamma_e = 1$.

shown in Figs. 3 and 4. However, the bidomain displacement is no longer zero. Figure 5 shows a plot of **b** with its spiraling geometry. Note that the magnitude of the bidomain displacement (Fig. 5) is much smaller than the monodomain displacement (Fig. 3), implying that the difference between the intracellular and extracellular displacements is small compared to the intracellular and extracellular displacements themselves. This distribution of the bidomain displacement [Fig. 5(b)] is qualitatively different than the distribution of monodomain strain (Fig. 4), and is largest where the fiber direction changes most rapidly. The bidomain displacement indicates where forces on integrins are greatest; Fig. 5(b) can be interpreted as a prediction of where integrins will cause mechanotransduction.

2. Shear

Monodomain displacement in isotropic tissue undergoing shear is shown in Fig. 6. The bidomain displacement is identically zero, the monodomain normal strain is zero, and the magnitude of the monodomain shear strain is $\frac{1}{2}$.

When anisotropic tissue with a fiber geometry given by Eq. (23) is sheared, plots of normal and shear strains (Fig. 7) are similar to when the tissue undergoes unixaial stretch. However, the normal strain is now small, and the shear strain contains small deviations from its isotropic value of $\frac{1}{2}$. The bidomain displacement is zero.

Figure 8 shows the bidomain displacement (and therefore the location of integrin activation and mechanotransduction) for tissue with unequal anisotropy ratios undergoing shear. The distribution of the displacement is similar to that in Fig. 5, but the magnitude is smaller. The monodomain displacement and strains are similar to Figs. 6 and 7.

B. Complex fiber geometry

Our second example fiber geometry is given by

$$\theta(X, Y) = \frac{\pi}{4}(-448X^6 + 240X^4 - 36X^2 + 1) \times (16Y^4 - 8Y^2 + 1), \quad (24)$$

which is distributed in the same region specified for Eq. (23), $-0.5 < X < 0.5$ and $-0.5 < Y < 0.5$ (Fig. 9). It is more complicated than in Fig. 2, and contains higher spatial frequencies.

1. Uniaxial stretch

For isotropic tissue the plot of monodomain displacement is the same as Fig. 3 (the fiber geometry plays no role when the tissue is isotropic). The bidomain displacement is zero.

For equal anisotropy ratios, the monodomain normal and shear strains are shown in Fig. 10. As before, the normal strain varies about a value of 1, and shear strain is small. The spatial distribution is different than in Fig. 4, reflecting the difference in fiber geometry. The bidomain displacement is zero.

For unequal anisotropy ratios, the bidomain displacement is no longer zero. The distribution of **b** is shown in Fig. 11; it is similar in magnitude but different in distribution than in Fig. 5.

2. Shear

When isotropic tissue with the fiber geometry shown in Fig. 9 undergoes shear, the monodomain displacement is identical to that shown in Fig. 6. The monodomain normal strain is zero, the monodomain shear strain is $\frac{1}{2}$, and the bidomain displacement is zero.

For equal anisotropy ratios, the monodomain displacement is like that shown in Fig. 6, and the bidomain displacement is zero. However, the monodomain strain shown in Fig. 12 has a different distribution than in Fig. 4, 7, or 10, indicating that both the fiber geometry and how the tissue is stretched are important for determining strain. As for all cases with equal anisotropy ratios, the bidomain displacement is zero.

When the tissue has unequal anisotropy ratios, the monodomain displacement and strain are similar to those shown in Figs. 6 and 12. The bidomain displacement is no longer zero and its distribution is shown in Fig. 13.

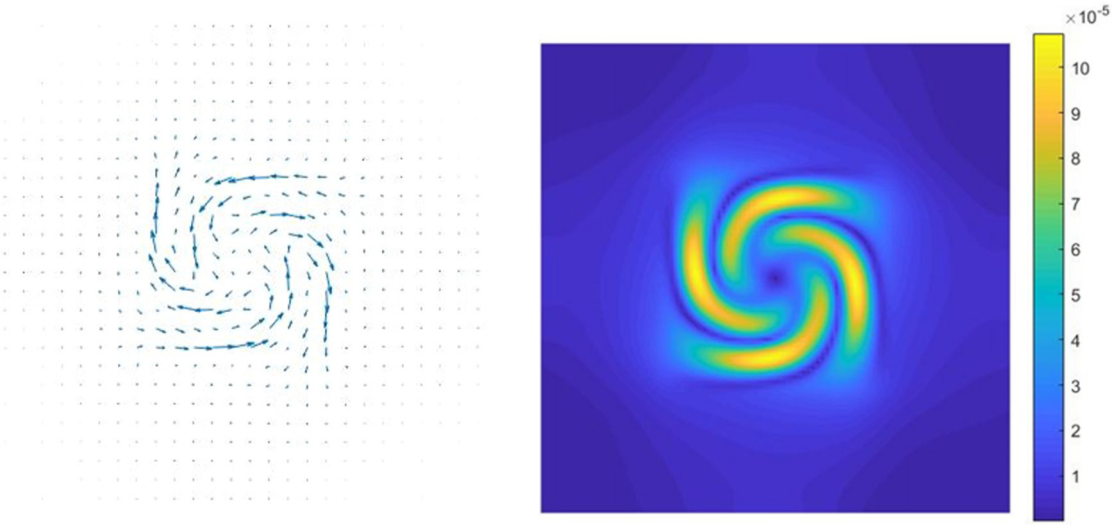

FIG. 8. (a) Bidomain displacement **b** in tissue with unequal anisotropy ratios under shear and (b) its magnitude $|\mathbf{b}|$. The fiber geometry $\theta(X, Y)$ is given by Eq. (23), boundary conditions were applied using $\psi = -\frac{X^2}{2}$, and $\gamma_i = 1$ and $\gamma_e = 0$. The length of the bidomain arrows in (a) is scaled differently than the length of the monodomain arrows in Fig. 6. The monodomain displacement is about 10 000 times larger than the bidomain displacement.

IV. DISCUSSION

We analyzed cardiac tissue using the mechanical bidomain model, which is a macroscopic mathematical model of mechanotransduction. The mechanical behavior of cardiac tissue becomes increasingly complex as we progress from an isotropic model, to equal anisotropy ratios, to unequal anisotropy ratios. For isotropic tissue the monodomain displacement is independent of fiber geometry; fiber direction has no influence (indeed no meaning at all) if the mechanical properties are isotropic: the same parallel and perpendicular to the fibers. Only in anisotropic tissue does fiber direction matter. In our examples, the monodomain strain is uniform, and depends on how the tissue is stretched (uniaxial stretch or shear). The bidomain displacement is zero. For equal anisotropy ratios the monodomain strain is more heterogeneous, but the inhomogeneities represent small deviations about the isotropic values. Our plots of strain (Figs. 4, 7, 10, and 12) may exaggerate the significance of these deviations, as the color scale extends over only a small range about the isotropic average value. The bidomain displacement remains identically zero. For unequal anisotropy ratios, the monodomain behavior changes only slightly, but the bidomain displacement is no longer zero, indicating a force on integrins. The distribution of $|\mathbf{b}|$ is qualitatively different than the distribution of strain (normal or shear). In particular, the strain caused by the curving fibers extends into the surrounding straight fibers to a greater degree than does the bidomain displacement.

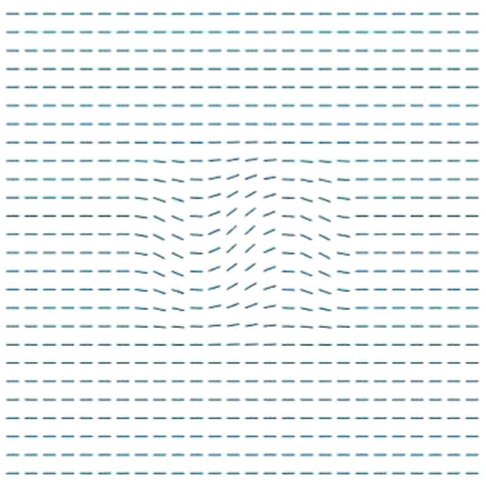

FIG. 9. The fiber distribution in a 2D sheet of cardiac tissue given by Eq. (24). X is horizontal and ranges from -1 to 1.

We have shown that unequal anisotropy ratios are critical for the bidomain displacement, and therefore for the distribution of forces on integrins and mechanotransduction. Does cardiac tissue have unequal anisotropy ratios? Most studies of cardiac biomechanics are based on monodomain models, so the anisotropic properties of the intra- and extracellular spaces are not measured individually. When Ohayon and Chadwick derived their monodomain model of cardiac tissue, they included an isotropic contribution corresponding to the extracellular collagen matrix, and an anisotropic contribution corresponding to the intracellular tension along the fibers caused by the interaction of actin and myosin [22]. If their model is recast in bidomain language, they would predict that cardiac tissue is more anisotropic in the intracellular space than in the extracellular space. The electrical properties of cardiac tissue are known to have unequal anisotropy ratios [23], so by analogy the mechanical properties may have unequal anisotropy ratios too. We do not have data to determine definitively if cardiac tissue has unequal anisotropy ratios. One contribution of our study is to suggest that experimental-

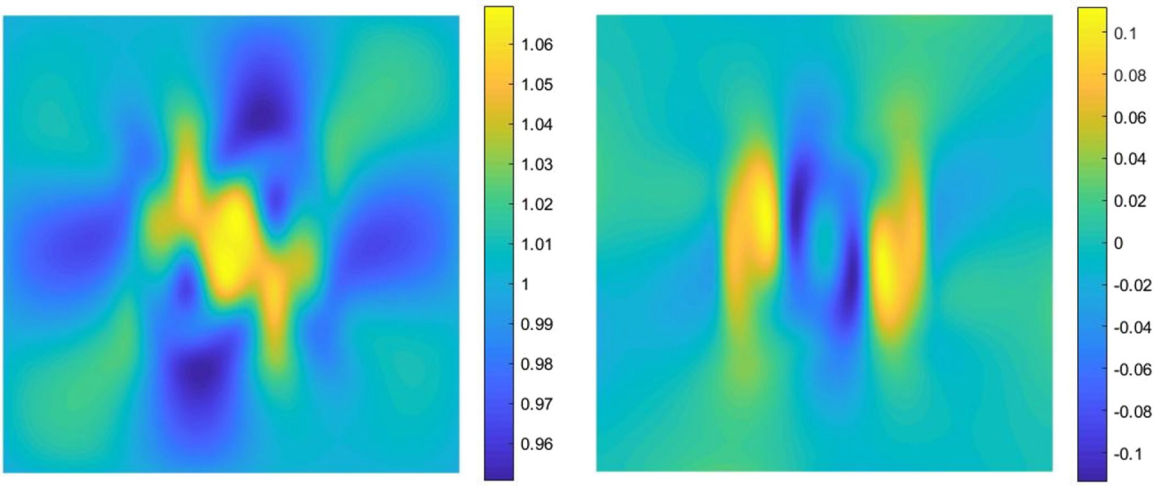

FIG. 10. Monodomain (a) normal strain and (b) shear strain for equal anisotropy ratios under uniaxial stretch. The fiber geometry $\theta(X, Y)$ is given by Eq. (24), boundary conditions were applied using $\psi = XY$, and $\gamma_i = \gamma_e = 1$.

ists should examine the mechanical properties and anisotropy in each space individually.

Our previous work indicates that bidomain displacements can occur near tissue boundaries [17]. We excluded boundary effects from this study by setting $\lambda = 0$ at the boundary. In general, bidomain displacements and integrin forces might occur both near tissue boundaries and in the bulk if the fibers are curving and the tissue has unequal anisotropy ratios. We speculate that other heterogeneities, such as a gradient in the intra- or extracellular shear modulus, that we did not consider here might also lead to bidomain displacements.

Fibers rotate and change direction in the heart [4,5]. However, our assumed fiber geometries in Figs. 2 and 9 are not meant to represent the realistic cardiac fiber geometry. Instead, we analyze two generic cases in order to highlight general principles. Experimentalists can create *in vitro* tissue samples having a user-specified fiber geometry [24,25], and our simulations might be experimentally tested using such techniques.

The bidomain model was derived based on the assumption that differences between intracellular and extracellular displacements cause forces on integrins and lead to mechanotransduction. Other monodomain studies have assumed that tissue stress or strain drives mechanotransduction, particularly during tissue growth and remodeling in the heart [6–9]. The distribution of monodomain strain and the distribution of bidomain displacement (integrin forces) are qualitatively

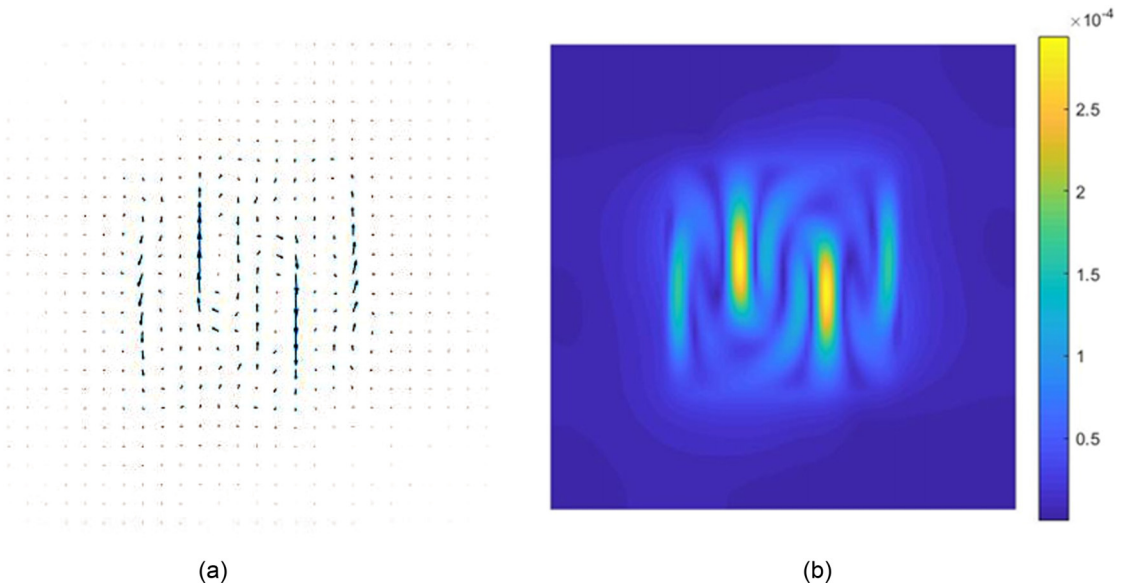

FIG. 11. (a) Bidomain displacement **b** in tissue with unequal anisotropy ratios under uniaxial stretch and (b) its magnitude $|\mathbf{b}|$. The fiber geometry $\theta(X, Y)$ is given by Eq. (24), boundary conditions were applied using $\psi = XY$, and $\gamma_i = 1$ and $\gamma_e = 0$. The length of the bidomain arrows in (a) is scaled differently than the length of the monodomain arrows in Fig. 3. The monodomain displacement is about 5000 times larger than the bidomain displacement.

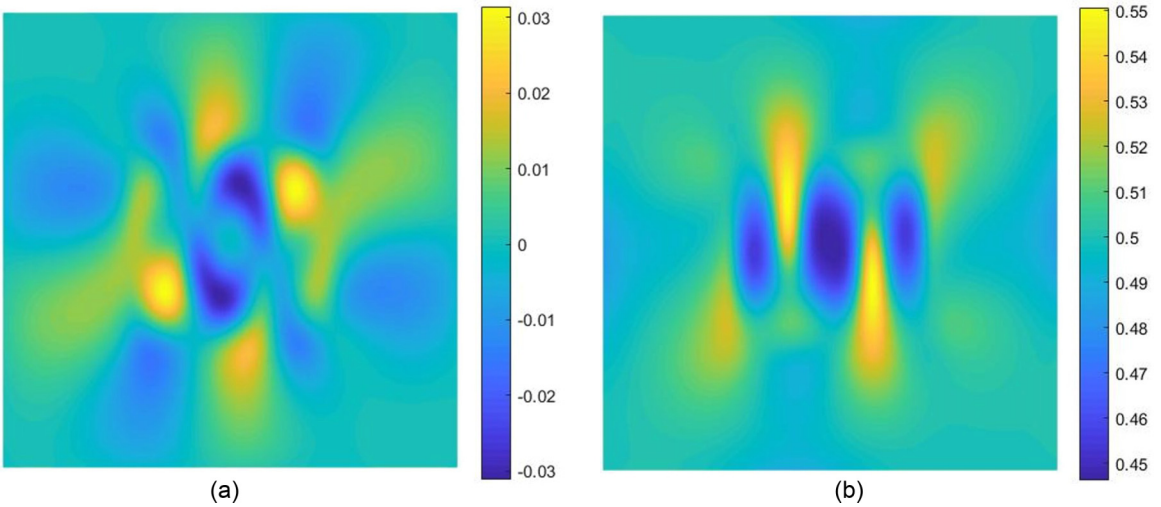

FIG. 12. Monodomain (a) normal strain and (b) shear strain for tissue with equal anisotropy ratios under shear. The fiber geometry $\theta(X, Y)$ is given by Eq. (24), boundary conditions were applied using $\psi = -\frac{X^2}{2}$, and $\gamma_i = \gamma_e = 1$.

different. Therefore, the distribution of cardiac growth and remodeling is different, depending on the underlying mechanism of mechanotransduction. In principle, one could measure the fiber distribution, compare strain and $|\mathbf{b}|$ in an experiment, and correlate them with the location of greatest tissue remodeling, and thereby distinguish between these two assumptions about the mechanism of mechanotransduction. Growth and remodeling of the heart is important in cardiac hypertrophy and heart failure. Therefore, a bidomain approach may be critical to understand these diseases.

The shear moduli of the intracellular and extracellular spaces, ν and μ, represent the isotropic part of the mechanical behavior. We assume that $\nu = \mu$. We repeated the calculations in Figs. 3 – 5 using $\nu = 0.5$, $\mu = 1$ and $\nu = 2$, $\mu = 1$. When the value of ν changed to 0.5, the magnitude of bidomain displacement was increased by nearly 25% with no significant changes in the spatial distributions of bidomain displacement, and monodomain normal and shear strains. Similar outcomes were observed in monodomain strains when the value of ν was changed to 2. However, the magnitude of bidomain displacement decreased by nearly 30% compared to the results shown in Fig. 5.

What we called the "additional Young's modulus" represents the increase in stiffness along the fiber axis compared to other directions and is a measure of the mechanical anisotropy. We examine cases in which γ_i and γ_e are either

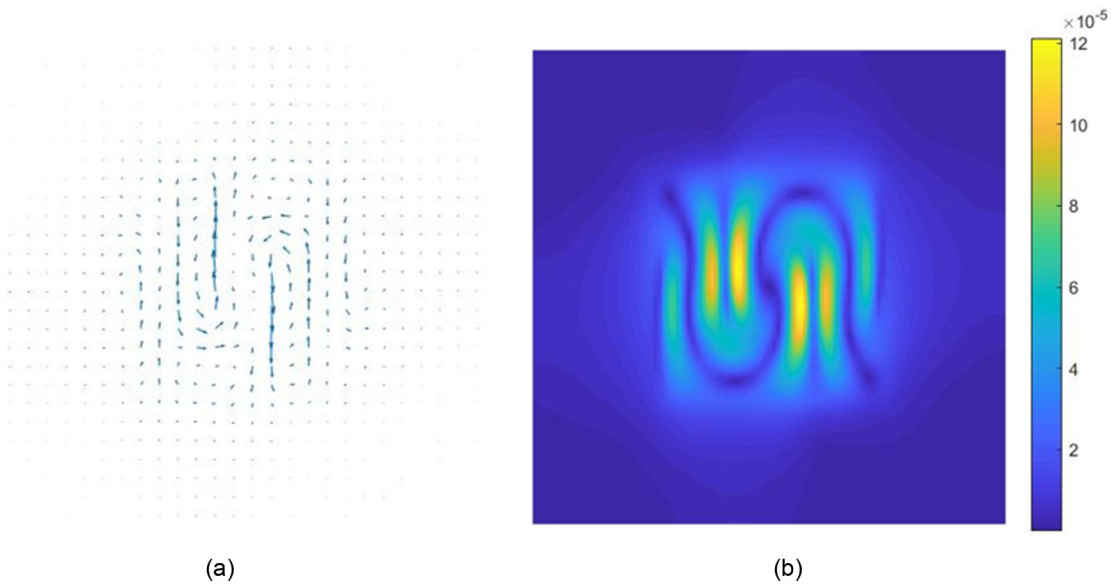

FIG. 13. (a) Bidomain displacement **b** in tissue with unequal anisotropy ratios when sheared and (b) its magnitude $|\mathbf{b}|$. The fiber geometry $\theta(X, Y)$ is given by Eq. (24), boundary conditions were applied using $\psi = -\frac{X^2}{2}$, and $\gamma_i = 1$ and $\gamma_e = 0$. The length of the bidomain arrows in (a) is scaled differently than the length of the monodomain arrows in Fig. 6. The monodomain displacement is about 10 000 times larger than the bidomain displacement.

zero or 1. In highly anisotropic tissue, $\frac{\gamma_i}{\nu}$ and $\frac{\gamma_e}{\mu}$ might be significantly greater than 1. We repeated the calculations in Figs. 4 and 5 using $\frac{\gamma_i}{\nu} = 10$, $\frac{\gamma_e}{\mu} = 10$ and $\frac{\gamma_i}{\nu} = 10$, $\frac{\gamma_e}{\mu} = 0$. We observed a large increase (≈600%) in the magnitude of bidomain displacement compared to the increase in monodomain normal (≈55%) and shear (≈400%) strains. Furthermore, when the anisotropy ratios are more different, the distribution of the magnitude of bidomain displacement becomes more localized.

The parameter ε represents the square of the ratio of the bidomain length constant, σ, to the tissue size, D. We do not know of data for σ in cardiac tissue. Using data from human embryonic stem cell colonies [26], Auddya and Roth [27] estimated σ is on the order of 150 μm. In the current study we considered $\sigma = 200$ μm and assumed the tissue size D is 20 mm, implying that $\frac{\sigma}{D}$ is $\frac{1}{100}$, and therefore $\varepsilon = 0.0001$. We repeated the calculation in Fig. 5 for $\varepsilon = 0.001$ and found that the magnitude of bidomain displacement increased in proportion to the value of ε, with no effect of ε on monodomain strains.

Our model is based on additional assumptions: (1) The tissue is at steady-state mechanical equilibrium. (2) Strains are linear. (3) The stress-strain relationship is linear. (4) The coupling between the intracellular and extracellular space is linear and can be represented by a spring constant K. (5) Both the intracellular and extracellular spaces are incompressible. (6) The tissue is two dimensional and undergoes plain strain.

Our results are not the first to examine the behavior of the mechanical bidomain model for curving fibers. Sharma and Roth [18] studied the case when the mechanical moduli are isotropic, but an active tension arising from the interaction of actin and myosin acts along the fiber direction. They found that bidomain behavior is localized to the region where fiber angle changes whereas monodomain behavior is widely distributed throughout the tissue. Also, they observed an increase in the magnitude of bidomain displacement and a more localized distribution when the value of ε is increased (monodomain behavior does not depend on ε).

Our calculation was motivated by the importance of unequal anisotropy ratios in the *electrical* bidomain model. Roth and Langrill Beaudoin [21] performed an electrical calculation that is analogous to our mechanical calculation. They applied a uniform electric field (rather than a uniform stretch) to tissue with curving fibers that had unequal ratios of electrical conductivity in the intracellular and extracellular spaces (rather than unequal ratios of mechanical moduli). They found a heterogeneous distribution of transmembrane potential (rather than integrin stretching) caused by the fiber curvature, which disappeared when the tissue had equal anisotropy ratios. The transmembrane potential had a spiral distribution reminiscent of the results shown in Fig. 5. Unequal anisotropy ratios have many implications for the electrical bidomain model [12] and might similarly have implications for the mechanical bidomain model beyond what we have discussed here.

In summary, we find that the mechanical bidomain model predicts unexpected behavior when the anisotropy of the mechanical moduli are different in the intracellular and extracellular spaces ($\frac{\gamma_i}{\nu} \neq \frac{\gamma_e}{\mu}$). If the differences between the intracellular and extracellular displacements drive mechanotransduction, then these differences can be predicted only by taking into account unequal anisotropy ratios. Our results could have implications for the study of growth and remodeling of cardiac tissue in the heart during diseases such as cardiac hypertrophy.

[1] Y. C. Fung, *Biomechanics: Mechanical Properties of Living Tissues* (Springer-Verlag, New York, 1981).

[2] J. D. Humphrey, *Cardiovascular Solid Mechanics: Cells, Tissues and Organs* (Springer, New York, 2002).

[3] A. D. McCulloch, Cardiac biomechanics, in *Biomedical Engineering Fundamentals*, edited by J. D. Bronzino (CRC Press, Boca Raton, FL, 2006).

[4] D. D. Streeter and W. T. Hanna, Circ. Res. **33**, 639 (1973).

[5] P. M. Nielsen, I. J. Le Grice, B. H. Smaill, and P. J. Hunter, Am. J. Physiol. **260**, H1365 (1991).

[6] W. Kroon, T. Delhaas, P. Bovendeerd, and T. Arts, Med. Image Anal. **13**, 346 (2009).

[7] P. H. M. Bovendeerd, J. Biomech. **45**, 872 (2012).

[8] R. C. P. Kerckhoffs, J. H. Omens, and A. D. McCulloch, Mech. Res. Commun. **42**, 40 (2012).

[9] M. Genet, L. C. Lee, R. Nguyen, H. Haraldsson, G. Acevedo-Bolton, Z. Zhang, L. Ge, K. Ordovas, S. Kozerke, and J. M. Guccione, J. Appl. Physiol. **117**, 142 (2014).

[10] C. S. Henriquez, Crit. Rev. Biomed. Eng. **21**, 1 (1993).

[11] N. G. Sepulveda, B. J. Roth, and J. P. Wikswo, Biophys. J. **55**, 987 (1989).

[12] B. J. Roth, in *Proceedings of the 28th Annual International Conference of the IEEE Engineering in Medicine and Biology Society, New York, 2006* (IEEE, Piscataway, NJ, 2006), p. 580.

[13] S. Puwal and B. J. Roth, Phys. Rev. E **82**, 041904 (2010).

[14] M. Brancaccio, E. Hirsch, A. Notte, G. Selvetella, G. Lembo, and G. Tarone, Cardiovasc. Res. **70**, 422 (2006).

[15] S. Israeli-Rosenberg, A. M. Manso, H. Okada, and R. S. Ross, Circ. Res. **114**, 572 (2014).

[16] B. E. Dabiri, H. Lee, and K. K. Parker, Prog. Biophys. Mol. Biol. **110**, 196 (2012).

[17] K. Sharma, N. Al-asuoad, M. Shillor, and B. J. Roth, J. Coupled Syst. Multiscale Dyn. **3**, 200 (2015).

[18] K. Sharma and B. J. Roth, Phys. Biol. **15**, 066012 (2018).

[19] S. P. Gandhi and B. J. Roth, Comput. Methods Biomech. Biomed. Eng. **19**, 1099 (2016).

[20] B. J. Roth, in *Cardiomyocytes: Methods and Protocols*, edited by G. R Skuse and M. C. Ferran (Humana, New York, 2015), Vol. 1299, p. 93.

[21] B. J. Roth and D. Langrill Beaudoin, Phys. Rev. E **67**, 051925 (2003).

[22] J. Ohayon and R. S. Chadwick, Biophys. J. **54**, 1077 (1988).
[23] B. J. Roth, J. Math. Biol. **30**, 633 (1992).
[24] A. Agarwal, Y. Farouz, A. P. Nesmith, L. F. Deravi, M. L. McCain, and K. K. Parker, Adv. Funct. Mater. **23**, 3738 (2013).
[25] N. Badie and N. Bursac, Biophys. J. **96**, 3873 (2009).
[26] K. A. Rosowski, A. F. Mertz, S. Norcross, E. R. Dufresne, and V. Horsley, Sci. Rep. **5**, 14218 (2015).
[27] D. Auddya and B. J. Roth, J. Phys. D **50**, 105401 (2017).